


Charge transfer mechanisms in DNA at finite temperatures: From quasiballistic to anomalous subdiffusive charge transfer

R. P. A. Lima^{1,*} and A. V. Malyshev^{2,3,†}

¹*GISC and GFTC, Instituto de Física, Universidade Federal de Alagoas, Maceió AL 57072-970, Brazil*

²*GISC, Departamento de Física de Materiales, Universidad Complutense, E-28040 Madrid, Spain*

³*Ioffe Physical-Technical Institute, St-Petersburg, Russia*

 (Received 27 January 2020; revised 21 June 2022; accepted 23 June 2022; published 31 August 2022)

We address various regimes of charge transfer in DNA within the framework of the Peyrard-Bishop-Holstein model and analyze them from the standpoint of the characteristic size and timescales of the electronic and vibrational subsystems. It is demonstrated that a polaron is an unstable configuration within a broad range of temperatures and therefore polaronic contribution to the charge transport is irrelevant. We put forward an alternative fluctuation-governed charge transfer mechanism and show that the charge transfer can be quasiballistic at low temperatures, diffusive or mixed at intermediate temperatures, and subdiffusive close to the DNA denaturation transition point. Dynamic fluctuations in the vibrational subsystem is the key ingredient of our proposed mechanism which allows for explanation of all charge transfer regimes at finite temperatures. In particular, we demonstrate that in the most relevant regime of high temperatures (above the aqueous environment freezing point), the electron dynamics is completely governed by relatively slow fluctuations of the mechanical subsystem. We argue also that our proposed analysis methods and mechanisms can be relevant for the charge transfer in other organic systems, such as conjugated polymers, molecular aggregates, α -helices, etc.

DOI: [10.1103/PhysRevE.106.024414](https://doi.org/10.1103/PhysRevE.106.024414)

I. INTRODUCTION

After the discovery of the DNA structure [1], its properties have been an object of an intensive interdisciplinary research. The interest in the DNA electronic properties increased considerably after it was put forward as a possible building block for the molecular electronics (see, for example, reviews [2,3] and references therein). Consecutive aromatic rings comprising the DNA double helix are coupled due to the overlap of their π orbitals, which determines different important electronic properties of the molecule [4]. The original conjecture was that these coupled states could provide a channel for the electric current, converting the DNA in a conducting nanowire, which was very promising for various applications. The DNA electrical properties have been measured experimentally revealing contradictory results, including insulating [5,6], semiconducting [7–10], and metallic [11–14] behavior. It was understood later that these differences were probably related to different experimental conditions, such as sample and contact types, measurement techniques, the DNA environment, etc. The investigation of the DNA involved studies of its optical [15–18], electronic [6,9,11,12,14,19–23], charge transport and transfer [4,5,7,8,10,13,24–59], and mechanical properties [60–63]. As far as the latter are concerned, one of the key mechanical phenomenon in the DNA is its denaturation, i.e., complete separation of the DNA strands, which was known to have a threshold-like character. That problem was successfully addressed theoretically in 1989 by Peyrard

and Bishop (PB) who proposed a model describing the denaturation as a phase transition in this quasi-one-dimensional (1D) system [60,61]. We note that the PB model is a particular case of a more general 1D model of a multicomponent nonlinear classical field. The latter was put forward in 1964 by Suris [64,65] who studied and analyzed its thermodynamic properties in detail, including the specific heat and correlation functions, and predicted that such a model can exhibit a phase transition. In the particular case of the PB model, the nonlinearity is introduced through the on-site Morse potential which accounts for the elastic energy related to the inter-strand hydrogen bond stretchings. In this case, the phase transition manifests itself in the divergence of these stretchings at the critical temperature, resulting in the denaturation phenomenon. The PB model has been widely used since then because of its success in the description of such an important biological process. Later, the model was extended by adding an electronic subsystem and considering a coupling of the lattice and electronic degrees of freedom [31,43,61], which allowed for taking into account the possible impact of phonons on the charge transfer processes.

Both purely ballistic transport [3,26] and the phonon-assisted transport and charge transfer [23,25,27–40] have been investigated thoroughly. In the latter case there are two opposite limits: Those of weak and strong electron-phonon interaction. In the former case the transfer is determined by the electron hopping assisted by phonons, thus, a disordered chain insulating at zero temperature can become conducting at nonzero temperature because of the thermal activation of the hopping mechanism (see, for example, Ref. [36] and references therein). However, a strong electron-phonon coupling can result in the formation of polarons which could

*rodrigo@fis.ufal.br

†a.malyshev@fis.ucm.es

determine the charge transfer [30–32,37,41,42]. A polaron, being an electron dressed by virtual phonons, has a larger effective mass than a bare electron [66,67], which is detrimental for the charge mobility. Although lower mobility is unfavorable for transport efficiency, electron-phonon interaction should be taken into account, provided it is relevant for the studied system properties. At zero temperature, a polaronic solution constitutes the ground state of the system. However, the contribution of the polaronic configuration to the partition function decreases at finite temperature, and it has been an essentially unexplored question, whether the set of configurations close to such a state is statistically meaningful. In this paper, we address this question, studying the polaron dynamics and its lifetime within a broad range of temperatures. We show that at nonzero temperatures the polaronic configurations are unstable and propose and analyze an alternative fluctuation-governed charge transfer mechanism which enables us to describe the charge transfer dynamics in all regimes at finite temperatures.

The paper is organized as follows. In the next two sections, we introduce the Peyrard-Bishop-Holstein (PBH) model which addresses a coupled electronic and DNA “lattice” dynamics and calculate its minimum energy configurations at $T = 0$. In the following sections, we address the system dynamics at non zero temperatures, both below and above the environment freezing point and consider two very different initial conditions. In Sec. IV, we use the traditional and somewhat artificial initial condition: The system in its polaronic state at zero temperature is subjected to the action of a heat bath, i.e., we address polaron dynamics during the chain thermalization (heating up) and analyze the polaron lifetime. In Sec. V, a more realistic initial condition is considered: An electron is injected in a thermalized DNA chain and the coupled system dynamics is studied. In the latter case, we discuss different nonpolaronic charge transfer mechanisms and regimes, in particular, quasiballistic, diffusive, mixed, and anomalous subdiffusive ones. Conclusions summarize the paper.

II. MODEL AND FORMALISM

In this section, we present the minimal set of equations of motion describing the dynamics of a system of N base pairs in the framework of the PBH semiclassical model: The electronic part is treated quantum-mechanically, while the lattice dynamics is treated classically using the Langevin approach (see Refs. [27,43,61] for more details). We use the following equation of motion of the n -th base-pair hydrogen bond stretching y_n (which describes the relative motion of the two base molecules of the pair):

$$\mu \frac{d^2 y_n}{dt^2} = -\frac{dV(y_n)}{dy_n} - \frac{dW(y_n, y_{n-1})}{dy_n} - \frac{dW(y_{n+1}, y_n)}{dy_n} - \mu\gamma \frac{dy_n}{dt} - \chi |\psi_n|^2 + f_n(t), \quad n = 1, 2, \dots, N, \quad (1)$$

where

$$V(y) = V_0(1 - e^{-\alpha y})^2 \quad (2)$$

is the on-site Morse potential and

$$W(y, y') = \frac{K(y - y')^2}{2} [1 + \rho e^{-\beta(y+y')}] \quad (3)$$

is the nearest-neighbor interaction potential which couples consecutive DNA base pairs. The real-space coordinate of the n th base pair is na_0 , with $a_0 \approx 3.4 \text{ \AA}$ being the chain “lattice” constant. In Eqs. (1)–(3), μ is the reduced mass of a base pairs (as in the bulk of the literature, we consider a homogeneous sequence of base pairs with the same reduced mass; we comment on possible impacts of the sequence inhomogeneity in Sec. V), γ is the friction constant, χ is the on-site electron-phonon coupling strength, while V_0 , α , K , ρ , and β are parameters characterizing the elastic potential energy. These parameters can be obtained through the comparison to the first-principle calculations [60,61,68] or experimental data [69,70].

Finally, the force $f_n(t)$ describes random action of the environment (thermal bath); it has the following statistical properties:

$$\begin{aligned} \langle f_n(t) \rangle &= 0, \\ \langle f_n(t) f_{n'}(t') \rangle &= 2\gamma \mu k_B T_0 \delta_{nn'} \delta(t - t'), \end{aligned} \quad (4)$$

where k_B is the Boltzmann constant and T_0 is the environment temperature. Such an approach is a microscopic model characterizing an aqueous (water-type) environment in terms of the collisions between the system and the “fast” reservoir molecules [27,71].

The original PB model [60] of the DNA “lattice” dynamics corresponds to Eq. (1) without the term $\chi |\psi_n|^2$ which accounts for the coupling to the electronic subsystem. The dynamics of the latter (within the framework of the Holstein approximation) can be described by the the following Schrödinger equation:

$$i\hbar \frac{\partial \psi_n}{\partial t} = -J(\psi_{n-1} + \psi_{n+1}) + U_n \psi_n, \quad (5)$$

where ψ_n is the charge carrier wave function at the n th site, J is the nearest neighbor electron coupling, and the last term with

$$U_n = \chi y_n \quad (6)$$

accounts for the interaction with the DNA “lattice,” where χ is the electron-phonon coupling constant.

As we demonstrate below, from the point of view of the relatively fast electronic subsystem, the interaction potential U_n is a random slowly varying on-site potential energy of the charge. However, relatively slow base pairs experience the electron-phonon coupling as an action of an external force which is proportional to the local electronic density [see the term $\chi |\psi_n|^2$ in Eq. (1)].

Some care should be taken while treating the interaction terms in Eqs. (1) and (5) because they correspond to the first-order expansion of the electronic energy with respect to the deformation of the π orbital due to the hydrogen bond elongation y_n . For large deviations from the equilibrium position such an approximation can fail. However, the Morse potential makes large negative values of y_n very unlikely, while large positive values of y_n , corresponding to broken bonds, give

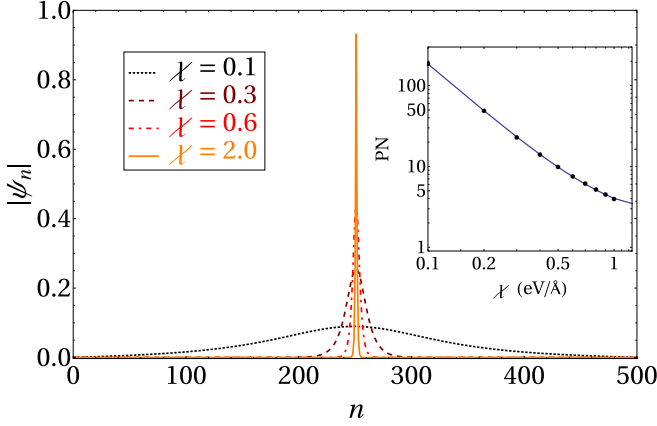


FIG. 1. Electronic wave function calculated for $T = 0$, $N = 500$, and different values of the coupling constant χ specified in the plot. The inset shows the dependence of the participation number on the coupling constant χ : Dots give the numerical result while the solid line is the best fit to the numerical data, given by the function $2.04 + 1.99 \chi^{-1.96}$.

rise to large potential barriers for the electron. Broken bonds are known to suppress the electronic transfer just like high potential barriers do, resulting in a qualitatively correct impact of large positive displacements on the charge transfer.

Computing the system dynamics requires specialized approach because of the presence of the stochastic term in the lattice equation of motion. In such a case, generic numerical calculation methods can become inaccurate while specialized algorithms of numerical integration of the stochastic differential equations [72,73] tend to give much more reliable results. Therefore, we used the **3o4s2g** algorithm: The third order Runge-Kutta method with four substeps and two random Gaussian number generated in each integration step.

III. POLARONIC SOLUTION AT $T = 0$

Hereafter, we use the following set of parameters (unless stated otherwise): $\mu = 300$ amu, $V_0 = 0.04$ eV, $\alpha = 4.45 \text{ \AA}^{-1}$, $K = 0.04 \text{ eV/\AA}^2$, $\rho = 0.5$, $\beta = 0.35 \text{ \AA}^{-1}$, $\gamma = 0.005 \text{ ps}^{-1}$, $\chi = 0.6 \text{ eV/\AA}$, $J = 0.1$ eV, which are typical values used in literature [31,43,61]. We restrict ourselves to the case of the homogeneous base sequence, which is the most favorable for the long-range charge transfer and transport and has been studied extensively (see, e.g., Refs. [26,59] and references therein). We comment on the possible impact of the differences in base pairs parameters in the Sec. V F.

The minimum energy configuration at zero temperature can be obtained by either iteration procedures [20,28] or by integrating Eq. (1) with an initial wave function $\psi_n(0)$ and displacements $y_n(0)$, which are similar in shape to the expected minimum configurations. Then, the drag term in Eq. (1) decreases the total energy of the system which finally relaxes to its ground state. In this study we used the latter method; the result is presented in Fig. 1 which shows the electronic wave function of the polaronic ground state for different values of the coupling constant χ .

To analyze the spacial extent of the electronic state quantitatively, we use the participation number (PN) of the state

defined as

$$P(t) = \left[\sum_{n=1}^N \psi_n^4(t) \right]^{-1}. \quad (7)$$

The physical interpretation of the PN is as follows. If the wave function is localized at N^* sites (let $N^* = \text{const} \leq N$), then its typical value at a site within its localization volume is on the order of $1/\sqrt{N^*}$ and the PN is on the order of N^* . So, it will remain finite in the thermodynamic limit $N \rightarrow \infty$. However, if the wave function is extended over the whole system, then the PN is on the order of the system size N diverging in the thermodynamic limit. Thus, the PN characterizes the spacial extent of the corresponding state and it is a very convenient quantity to study localization and delocalization properties and phenomena. Speaking more strictly, the PN gives the number of sites which provide the main contribution into the normalization of the wave function, i.e., the number of sites where the wave function has appreciable amplitude. The latter is very important for the electron-phonon interaction too because the coupling term in the lattice equation of motion (1) is proportional to the local electronic density $|\psi_n|^2$, so the coupling is significant only at the sites where the wave function has appreciable amplitude. In particular, significant negative displacements y_n (characteristic for a polaronic configuration) can only exist at such sites and therefore the PN can characterize also the size of a polaron if the latter exists. If the extent of the wave function increases, then the electron-phonon coupling is reduced [74], which can manifest itself in the breakup of the polaron, as we show below.

The dependence of the polaronic ground state PN on the coupling constant χ is shown in the inset of Fig. 1. As expected, the size of the polaron reduces as the coupling increases. Simple analytical estimates of the polaron characteristic parameters can be obtained by the variational calculation, using Gaussians for both the polaronic deformation y_n and the charge wave function ψ_n in the continuous limit:

$$\begin{aligned} y(x) &= -d_p \exp\left(-\frac{x^2}{a_p^2}\right), \\ \psi(x) &= \frac{1}{\pi^{1/4} a_p^{1/2}} \exp\left(-\frac{x^2}{2a_p^2}\right), \end{aligned} \quad (8)$$

where x is the continuous coordinate along the chain. In this case the optimized polaronic deformation amplitude d_p , the polaron energy E_p , and its “size” a_p are as follows:

$$\begin{aligned} d_p &= \frac{\chi^3}{8\sqrt{2\pi} J V_0^2 \alpha^4}, \\ E_p &= \frac{\chi^4}{64\pi J V_0^2 \alpha^4}, \\ a_p &= \frac{4\sqrt{2\pi} J V_0 \alpha^2}{\chi^2}, \end{aligned} \quad (9)$$

while the corresponding polaronic wave-function participation number P_0 is

$$P_0 = \sqrt{2\pi} a_p = \frac{8\pi J V_0 \alpha^2}{\chi^2}. \quad (10)$$

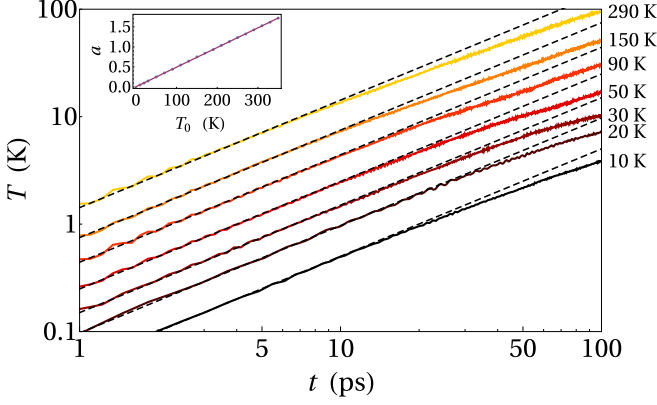


FIG. 2. Time dependence of the averaged temperature T of the chain calculated for different bath temperatures T_0 indicated in the plot (the chain was initially at rest: $y_n(0) = \dot{y}_n = 0$). Straight dashed black lines are best fits to the data for $t \leq 10$ ps. The dependence of the slope a of these lines on the bath temperature T_0 is shown in the inset.

For the used set of parameters the above estimate of the PN evaluates to $P_0 \approx 1.99 \chi^{-2}$ which is in very good agreement with the numerical result $2.04 + 1.99 \chi^{-1.96}$ (see the inset of Fig. 1). The discrepancy at large values of the coupling constant χ is expectable: As the interaction increases, the polaron size shrinks down to few lattice constants and the continuous approximation becomes inadequate.

Equations (9) give the following estimates of the polaronic deformation amplitude, polaron energy, and its PN:

$$d_p \approx 0.1 \text{ \AA}, \quad E_p \approx 10 \text{ meV}, \quad P_0 \approx 5.5 a_0, \quad (11)$$

which are also in very good agreement with the values obtained numerically. Based on the value of the polaron energy E_p , one might assume that the polaron can exist up to temperatures on the order of $E_p/k_B \sim 100$ K, which does not prove to be the case as we show below.

IV. POLARON DYNAMICS DURING THE CHAIN THERMALIZATION

In this section, we study the polaron dynamics *during* the chain thermalization. First, to obtain the characteristic timescale of the chain thermalization process itself, we address the dynamics of the DNA “lattice” uncoupled from the electronic subsystem (which corresponds to the original PB model). Hereafter, the chain length $N = 100$ is used unless otherwise stated.

We found that the thermalization process is described by a simple exponential law for the current chain temperature T as a function of time:

$$T(t) = T_0(1 - e^{-t/\tau_0}), \quad (12)$$

where τ_0 gives the timescale of the heating process. The above dependence can be verified numerically. Figure 2 shows the time dependencies of the configuration-averaged chain temperature T for different bath temperatures T_0 . The temperature of the chain is estimated using the virial theorem, which relates the kinetic energy of the system with its temperature,

$E_{\text{kin}} = N k_B T/2$. By fitting the formula

$$T(t) \approx \frac{t}{\tau_0} T_0, \quad t \ll \tau_0, \quad (13)$$

to the initial linear part of the curves in Fig. 2, one obtains the slope $a = T_0/\tau_0$ and therefore the characteristic heating time $\tau_0 \approx 204$ ps. The inset of the figure shows the expected linear dependence of the slope on the bath temperature.

The parameter τ_0 can be estimated analytically by considering the energy transferred to the forced oscillator system. During the initial phase of heating the damping is negligible ($t \ll 1/\gamma$) and the typical displacement is small, so that the interaction potential (3) can be neglected too, then a harmonic oscillator model of the Morse potential (2) is applicable. In such a simplified case the transferred energy at the time t to the forced oscillator is given by [75]

$$E_T = \frac{1}{2M} \left| \int_{-\infty}^t \sum_n^N f_n(t') e^{i\omega t'} dt' \right|^2, \quad (14)$$

where $M = N\mu$ is the total reduced mass and ω is the frequency of the harmonic oscillator. Using the statistical properties of the random force $f(t)$, given by Eq. (4), one can calculate the transferred energy as

$$E_T = N k_B T_0 \gamma t.$$

Otherwise, the energy of an oscillator system can be obtained as twice the kinetic energy: $2E_{\text{kin}} = N k_B T(t) = N k_B T_0 t/\tau_0$. Equating the two results gives the estimate of the parameter τ_0 as

$$\tau_0 = \frac{1}{\gamma} = 200 \text{ ps},$$

which is in a very good agreement with the result obtained numerically from the dependencies shown in the Fig. 2: $\tau_0 \approx 204$ ps.

Second, we consider the complete system dynamics using the polaronic solution at zero temperature localized at the center of the chain (obtained as described in the previous section) as the initial condition. We assume also that at $t \geq 0$ the system is subjected to the action of the heat bath with the temperature T_0 . Although the physical relevance of this initial condition could be questioned, it has been widely used in the literature (see Refs. [20,27,49,50] and reference therein) and it guarantees the existence of a polaron in the system at the initial moment of time. If the polaronic solution is relevant (stable), then one would expect it to survive the complete thermalization process, until the system reaches the temperature of the bath.

Our calculations show that the polaron falls apart during the thermalization; to account for that we introduce the polaron lifetime, defining it as the polaron breakup or delocalization time τ_d . Below we study this quantity as a function of the bath temperature T_0 and address also the temperature of the DNA chain at $t = \tau_d$, i.e., at the moment of the polaron breakup.

Figure 3 demonstrates an example of the system dynamics for $T_0 = 80$ K. The upper and middle panels show the spatiotemporal maps of bond stretchings y_n and the probability density $|\psi_n|^2$, respectively. The system starts from a polaronic

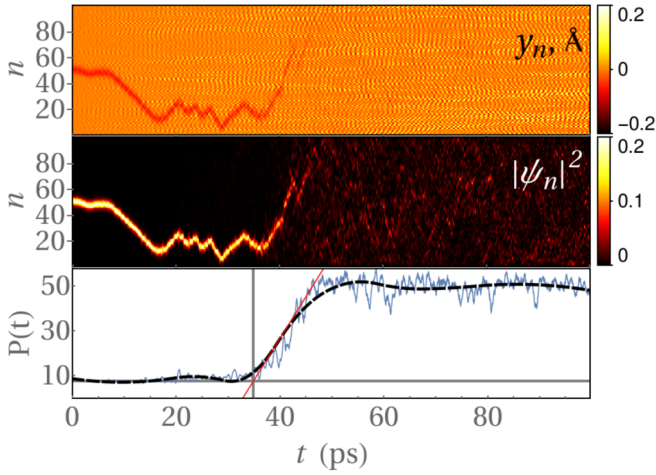


FIG. 3. Maps of the spatiotemporal evolution of the hydrogen bond stretchings y_n (upper panel) and the probability density $|\psi_n|^2$ (middle panel). The polaron was initially located at the center of the chain, at $t = 0$ the system was coupled to a heat bath with the temperature $T_0 = 80$ K. Lower panel shows the time dependent participation number $P(t)$ (solid blue line) and its smoothed version $\bar{P}(t)$ (dashed black line). Solid red and horizontal gray lines are used to calculate the polaron breakup time τ_d (see text for details); the latter is marked by the vertical gray line.

state which is characterized by the highly localized negative stretching and wave function. Within the initial part of the trajectory (in the time range $t \lesssim 40$ ps), there is a clear correspondence of the high electronic density and negative lattice distortion, which is a fingerprint of a polaron. As the system is heated up, the amplitude of the random oscillations grows and when it becomes comparable to the polaronic deformation amplitude d_p the polaron becomes unstable. As can be seen from the figure, at $t \approx 40$ ps the polaron finally breaks up: The wave function delocalizes and spreads over the whole chain. The lower plot clearly shows the transition between two regimes of the PN dynamics: The polaronic solution has $PN \approx 7$ for $t \lesssim 40$ ps, while the final delocalized state has $PN \approx N/2 = 50$.

To estimate the polaron lifetime or the delocalization time τ_d we use several auxiliary quantities proceeding as follows. First, we calculate the integrated participation number:

$$I(t) = \int_0^t P(t') dt', \quad (15)$$

which is interpolated using a sparse mesh of points giving a smooth function of time $I_{\text{int}}(t)$, whose derivative $\bar{P}(t) = \dot{I}_{\text{int}}(t)$ is a smoothed version of the function $P(t)$. Black dashed line in the lower panel of Fig. 3 shows the smooth function $\bar{P}(t)$. We define the polaron delocalization time τ_d by the following equation:

$$\dot{P}(t_i) = \frac{\bar{P}(t_i) - \bar{P}(0)}{t_i - \tau_d},$$

where t_i is the inflection point of $\bar{P}(t)$ in the transition region, in which the participation number starts growing fast, i.e., t_i is the point where the first derivative $\dot{\bar{P}}(t)$ is maximum. Thus, τ_d is determined by the intersection of the linear interpolation

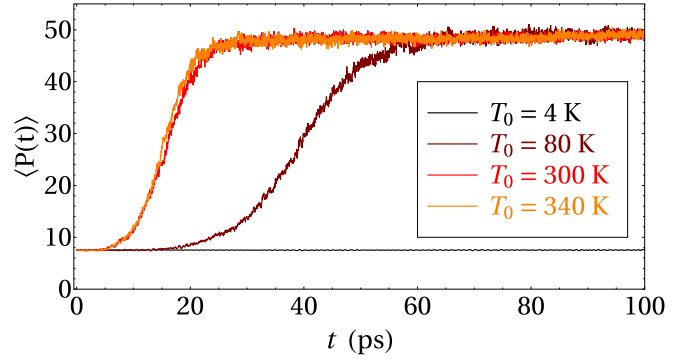


FIG. 4. Time dependence of the ensemble averaged participation number $\langle P(t) \rangle$ calculated for different bath temperatures indicated in the plot. Results are obtained using the polaronic solution as the initial condition.

of the $\bar{P}(t)$ in the vicinity of the inflection point (see the solid red line in the lower panel of Fig. 3) and the line giving the initial polaron size $\bar{P}(0)$ (shown by the horizontal dark gray line).

The time evolution of the ensemble averaged participation number $\langle P(t) \rangle$ for different bath temperatures T_0 is shown in Fig. 4 (hereafter, $\langle \dots \rangle$ denote ensemble averaging; for each temperature, 100 trajectories were used to calculate the average). The figure suggests that the polaron lifetime becomes shorter for higher temperatures, as can be expected: As Fig. 2 and Eq. (12) show, the chain heats up faster at higher bath temperatures and therefore the characteristic amplitude of random oscillations grows faster resulting in faster breakup of the polaron. Figure 5 shows the dependence of the polaron lifetime on the bath temperature T_0 , which turns up to be a power law one (see the inset demonstrating the best power law fit to the data in double logarithmic scale).

Using the thermalization timescale τ_0 and the obtained polaron lifetime power law dependence on the bath temperature T_0 , it is straightforward to calculate the chain temperature T_d at $t = \tau_d$, i.e., at the moment when the polaron breaks up and the electron wave function starts extending over the

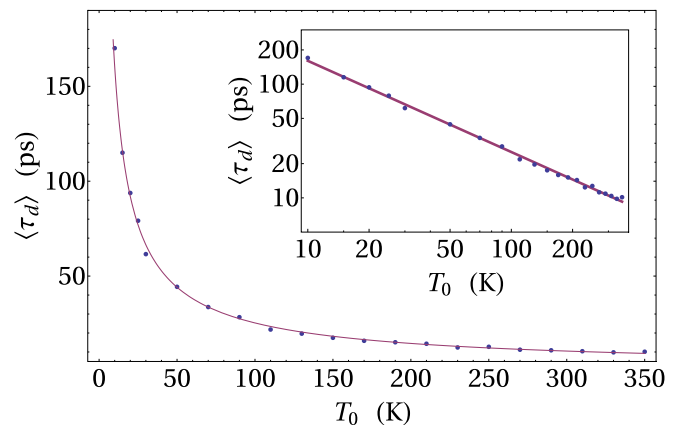


FIG. 5. Ensemble averaged polaron lifetime $\langle \tau_d \rangle$ as a function of the bath temperature T_0 . Dots represent numerical results while solid lines give the best fit to the numerical data. It can be seen from the inset that the data follows the power law (with the exponent of approximately -0.8).

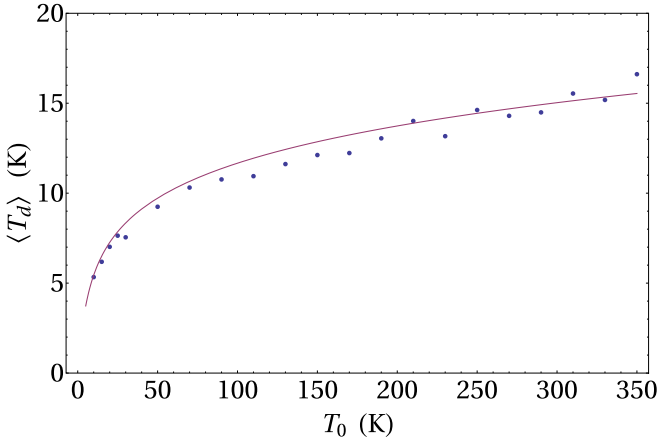


FIG. 6. Ensemble averaged temperature of the chain $\langle T_d \rangle$ at the polaron breakup time $\langle \tau_d \rangle$ as a function of the bath temperature T_0 . Dots show numerical result while the solid line—the theoretical estimation of $T(\tau_d)$ obtained using Eq. (12) and the best fits from Figs. 2 and 5.

whole chain. The result is shown in Fig. 6, where the points represent the computed averaged chain temperature at $t = \tau_d$ as a function of the bath temperature T_0 . The solid line shows the theoretical estimation of $T_d = T(\tau_d)$ according to Eq. (12) in which the best fit parameters from the previous calculations are used. The two results are in good agreement with each other, which indicates that our considerations are self consistent. Our findings suggest that the polaron breaks up for not so low temperatures ($T_0 > 10$ K). Moreover, it breaks up long before the target chain thermalization temperature T_0 is reached because $T_d < T_0$ and $\tau_d < \tau_0$ for all considered cases. We conclude therefore that the polaronic configuration can hardly be expected to be a relevant state of the system in the studied temperature range within the framework of the PBH model. We comment in more detail on the low temperature regime dynamics in Sec. VC.

Finally, we point out that in the current section we considered a very artificial scenario in which a polaron existed initially. Nevertheless, we found that polarons are not stable even under such favorable conditions. Below we address a more realistic initial condition.

V. DYNAMICS OF AN ELECTRON IN A THERMALIZED LATTICE

In this section we address the dynamics of a charge injected in a thermalized chain which has the temperature of the heat bath: $T = T_0$. Such an initial condition can be realized when an electron belonging to the DNA environment hops to one of the nucleotides. If the polaronic solution is relevant and stable, then one would expect that the system would evolve toward it.

To model this scenario we proceed as follows. We solve the Langevin equation for the molecule chain mechanical subsystem (decoupled from the electronic one) until it reaches thermal equilibrium at the bath temperature T_0 . Then, at $t = 0$ an electron is created at the center of the chain ($n = N/2$) in the form of the δ -function wave packet and the dynamics of the full coupled system is studied (further we argue that

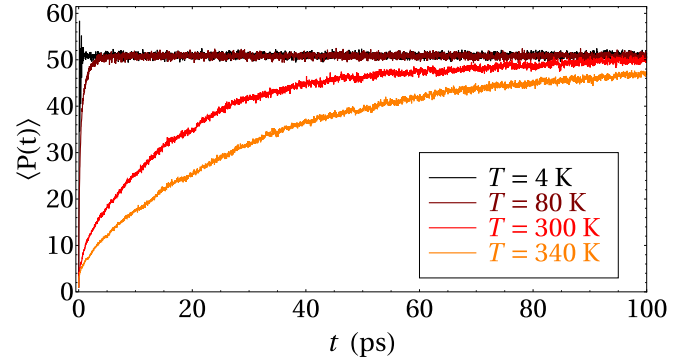


FIG. 7. Time dependence of the average participation number $\langle P(t) \rangle$ calculated for different thermalized chain temperatures T indicated in the plot. These results were obtained using an electron injected at $n = 50$ in the thermalized chain as the initial condition. For every temperature, 100 trajectories were used to calculate the average.

choosing a different initial site would have almost no effect on final results). Below we address such dynamics for different temperatures and demonstrate that there exist qualitative different regimes of the charge density dynamics. To this end, we study the time evolution of the the PN characterizing the spacial extent of the wave function, as well as the typical system trajectories to get insight into the underlying mechanisms of the electronic density dynamics.

Figure 7 shows the time dependence of the ensemble averaged participation number for different temperatures. The figure shows no traces of the polaron formation for all temperatures: The PN grows to its maximum value, which corresponds to the charge density distributed almost homogeneously over the whole sample. As can be seen from the figure, the wave function expands faster for lower temperatures, which may seem counter intuitive. Indeed, this trend is just the opposite compared to that observed in the previous section where we showed that the polaron lifetime (delocalization time) is larger for lower temperatures.

To explain the increase of the wave-function expansion time with temperature we note that, because of the structure of the interaction term (6), lattice vibrations result in a random time-dependent potential for the charge. The amplitude of this on-site potential can be characterized by the temperature dependent typical value of the stretching y_n which increases with the temperature making the system more “disordered,” which slows down the charge dynamics.

All the above arguments are based on the dynamics of the PN which is an integrated characteristics of the system. Therefore, such considerations can and actually do overlook important details of the charge density dynamics. To get an insight into the latter, we proceed by studying particular typical trajectories for different temperatures, to pinpoint important characteristic features of the system dynamics in different regimes manifesting themselves at different temperatures.

A. Low temperatures: Quasiballistic propagation

First, we address the case of very low temperatures. Figure 8 shows results of the calculation of one particu-

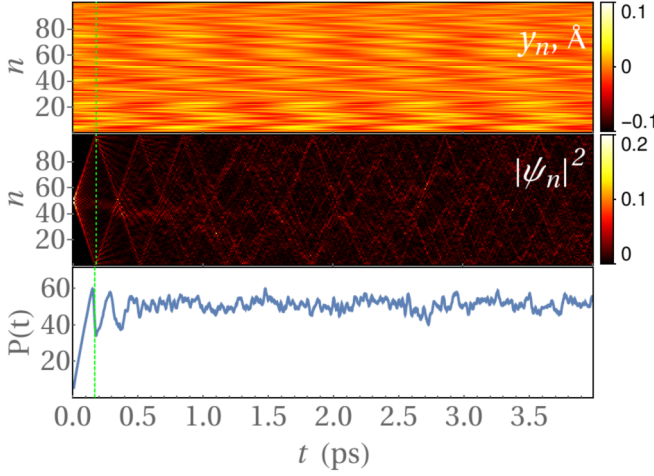


FIG. 8. Maps of the spatiotemporal evolution of the hydrogen bond stretchings y_n (upper panel) and the probability density $|\psi_n|^2$ (middle panel). The lower panel shows the time dependence of the participation number $P(t)$. The vertical green dotted line gives the time of flight (see text for details). All results are calculated for the case when an electron is injected into the chain thermalized at $T = 4$ K.

lar trajectory for $T = 4$ K. Upper and middle panels show the spatiotemporal maps of the bond stretchings y_n and the probability density $|\psi_n|^2$, respectively. The upper panel demonstrates that the typical bond stretching is very small: On the order of $0.05 \text{ \AA} \ll 1/\alpha$. In this case, the Morse potential can be approximated by the parabolic one:

$$V(y_n) \simeq V_0 \alpha^2 y_n^2, \quad (16)$$

which has the period of oscillation $2\pi \sqrt{\mu/2V_0\alpha^2} \approx 0.88$ ps. Patterns with such a period are clearly observed in the upper panel of the figure. Note also the evident absence of the influence of the electronic density on the lattice dynamics: It is qualitatively the same during the initial phase when the electron is more localized and during the following phase when the electronic density is extended over the whole chain. Besides, the whole displacement pattern is very homogeneous showing no outstanding features (below we will contrast this very uniform pattern to those characterized by large fluctuations at higher temperatures).

The middle panel of Fig. 8 shows typical features of the ballistic propagation for $t < 0.5$ ps: The straight tracks crossing the whole sample. The existence of such a pattern can be explained as follows. Using the dispersion relation for a one-dimensional ideal chain, we can calculate the group velocity:

$$v_g(k) = \frac{2a_0J}{\hbar} \sin\left(\frac{\pi k}{N+1}\right), \quad k = 1, 2, \dots, N, \quad (17)$$

where k is the state number. The initial δ -function wave packet projects almost uniformly over the eigenstates with odd values of k . The fastest modes belong to the center of the energy band (those having $k \approx N/2$); they have the group velocity $v_g = 2a_0J/\hbar$ of about $300 a_0/\text{ps}$, and therefore travel over a half of the chain in about 0.17 ps (the vertical green line in Fig. 8 gives this timescale). Note that the latter time of flight

is about six times smaller than the characteristic oscillation period of 0.88 ps, so for these states the electron-phonon coupling reduces to interaction with a virtually static disorder. These faster states are less affected by disorder than slower edge states (those with $k \sim 1$ or $k \approx N$) because of the motion averaging effect: The faster a state is propagating the better it is averaging the disorder, making the latter effectively weaker. The lower panel of Fig. 8 shows the dynamics of the PN which is also growing very fast, reducing the typical wave-function amplitude and consequently the electron-phonon coupling even further [74]. Therefore, the part of the wave packet corresponding to the faster band-center states travels ballistically during the first phase of the propagation. When it reaches the hard boundary of the chain it gets reflected and travels backwards, which can clearly be seen in the Fig. 8. The ballistic propagation manifests itself also in the characteristic interference fringes of the PN (see the lower panel of the figure at $t < 0.5$ ps).

Note that even in the current case of very low temperatures, when the oscillation period is the shortest possible (about 0.88 ps), all characteristic lattice timescales are much larger than those of the electronic subsystem: The average group velocity \bar{v}_g is on the order of $200 a_0/\text{ps}$, so the corresponding timescale is $a_0/\bar{v}_g \sim 0.005$ ps. Thus, the lattice is unable to adapt itself to fast changes of the electronic density and, for example, a polaron can not form. Besides, amplitudes of the lattice vibration are small and very homogeneous, so they do not provide high potential barriers for the charge carrier, which could scatter it back efficiently as in the case of higher temperatures (see below).

To further analyze charge transfer mechanism, we calculate also the time evolution of the wave packet width, i.e., the standard deviation of the electronic density for a given trajectory, defined as follows:

$$s(t) = \sum_n (n - x(t))^2 |\Psi_n(t)|^2, \quad (18)$$

where $x(t)$ is the wave packet centroid position:

$$x(t) = \sum_n n |\Psi_n(t)|^2. \quad (19)$$

Figure 9 shows the time dependence of the ensemble averaged packet width $\sigma(t) = \langle s(t) \rangle$ calculated for a chain of $N = 1000$ sites at $T = 4$ K. The packet width saturates at long times when the packet expands over the whole chain—this is just a finite size effect. The best power law fit for short times, given by the red line in the figure, has the exponent very close to unity. Thus, we conclude that at very low temperatures a substantial part of the charge wave packet can expand ballistically over distances on the order of a hundred lattice constants. Similar results were reported recently in Ref. [51], where ballistic propagation of Frenkel excitons in molecular aggregate systems at low temperatures was discussed.

B. Intermediate temperatures: Diffusive regime

Next, we consider the system dynamics in the regime of low to intermediate temperatures. Results of our calculation of one particular system trajectory are presented in Fig. 10

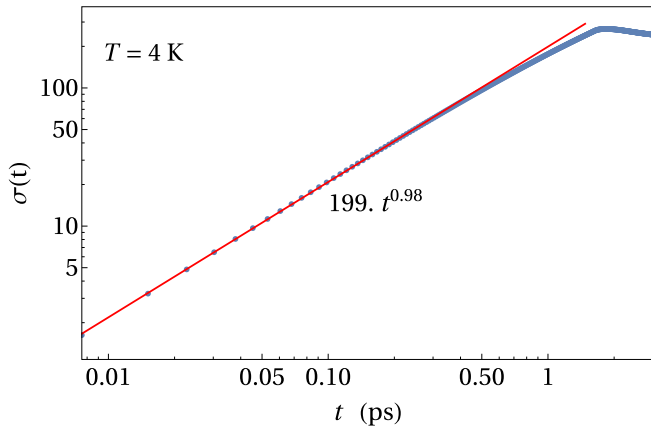


FIG. 9. The time dependence of the ensemble averaged standard deviation of the electronic density (packet width) calculated for a chain of $N = 1000$ sites and $T = 4$ K. Solid red line gives the best power law fit to the data within the region $t < 0.3$ ps. The best fit function is shown next to the line.

which has the same layout as Fig. 8. As in the previous case, the upper plot of the bond stretchings shows clear traces of oscillatory motion but the typical value of the stretching is about 0.2 \AA now. In this case, the Morse potential is not quadratic anymore and the characteristic period is somewhat larger than that of the harmonic potential approximation used above. More importantly, the y_n pattern is not as homogeneous as before: there are clearly visible long-living stronger fluctuations of the whole chunks of the chain (see the stripes with light yellow parts marking large positive stretchings of chunks of adjacent molecules). For example, see the strong oscillatory fluctuations about $n \approx 35$ and $n \approx 55$: Their periods are larger than that of the harmonic oscillation (we mark the harmonic half period of 0.44 ps by the vertical green line in the figure for the reference). When such an oscillating chunk of the lattice is stretched it represents a sufficiently high potential barrier for an electron due to the interaction term Eq. (6). Note how the expanding wave packet is reflected back by these potential

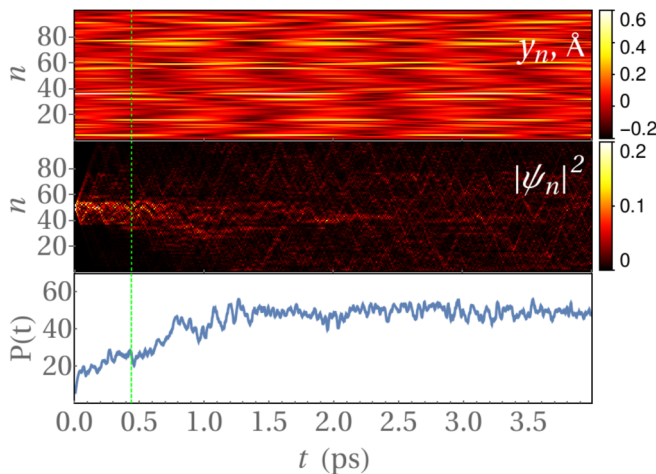


FIG. 10. Same as in Fig. 8 but for $T = 80$ K and the vertical green line gives the harmonic oscillation half period of 0.44 ps (see text for detail).

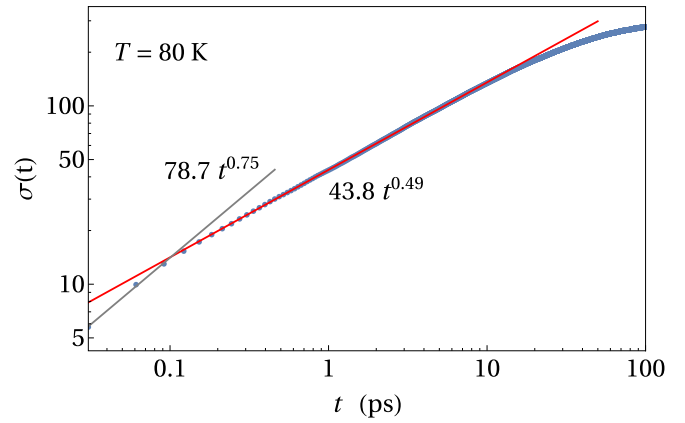


FIG. 11. Same as in Fig. 9 but for $T = 80$ K. Solid red line gives the best power law fit to the data within the region $0.1 < t < 10$ ps while the solid gray line—in the region $t < 0.1$ ps.

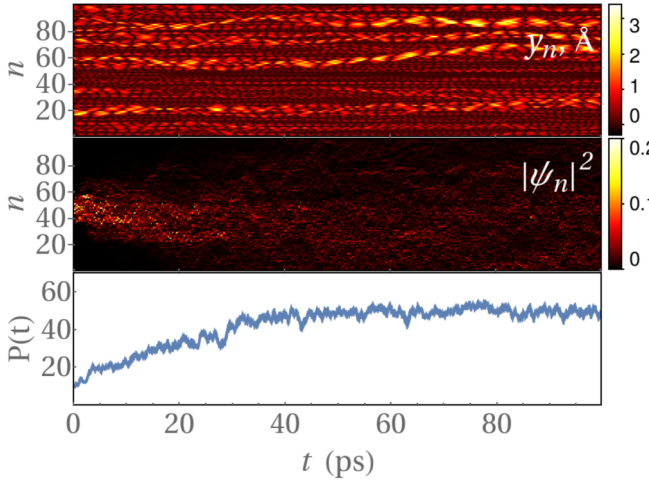
barriers (see the middle panel) and remains localized between them for some appreciable time. So, as long as these barriers are high the charge is largely confined between them. However, during the other part of the oscillation period when the bond stretchings shrink and potential barriers practically disappear, the charge density leaks out and propagates further.

Therefore, the chain oscillation period sets a natural timescale for the charge propagation. It is important that the system is far from the phase transition point at such temperatures and therefore it can be characterized by the finite and well defined size and timescales of oscillations of either base pairs or finite chunks of them. These oscillations rise and lower potential barriers for an electron; the phases of the oscillations are random, so the charge transfer mechanism is very similar to that of a random walk resulting eventually in diffusive regime of the charge dynamics at sufficiently long times, which can be seen in the Fig. 11 demonstrating the diffusive growth of the wave packet width.

C. On the applicability of the PBH model for temperatures below the environment freezing point

We have considered the system dynamics at relatively low temperatures of the environment forming the thermal bath. In the case of DNA and other organic molecules this environment is typically water based, so we have been studying these systems for temperatures well below the freezing point of the medium they are embedded into. There are several concerns related to the latter circumstance we will discuss.

For temperatures close to the medium melting point (usually about 0°C) the typical stretching is on the order of an \AA (results not shown here). Recall that in the case of DNA the stretchings y_n are the elongations of H-bonds between the base molecules forming the two DNA strands. Thus, these elongations represent relative displacement of large base molecules. If the environment is a fluid and fast enough, then it can easily adapt itself to relatively slow changes in base pair configuration. However, below the freezing point the medium is glassy and it can hardly support such large displacements of bulky objects embedded into it. Therefore, the applicability of the PBH model for such temperatures can be questioned.

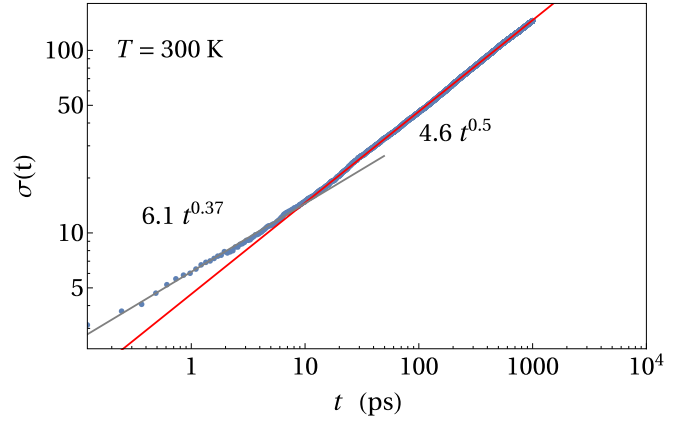
FIG. 12. Same as in Fig. 8 but for $T = 300$ K.

Unphysically large displacements do not occur at low temperatures. See, for example, the upper panel of Fig. 10 from which the characteristic bond stretching at $T = 80$ K can be estimated to be on the order of 0.2 \AA . However, there is another concern: The stochastic term in the Langevin equation, which models the action of the bath is uncorrelated. This is reasonable for a very fast liquid environment but does not seem to be adequate for a glassy matrix in which the local configuration of each base pair molecule is random but frozen and therefore correlated at least in time. Such a random local environment introduces a *static* disorder into the system, resulting in characteristic energy structure of localized states (see, e.g., Refs. [76–81]), while the action of the bath can be considered as the interaction with phonons of the glassy host. We believe that the latter model is more realistic for the considered systems at low temperatures. We note finally that such a model of phonon-assisted transfer has been used very successfully for describing quantitatively various properties of molecular aggregates at low temperatures (see, for example, Ref. [82–84] and references therein) as well as some aspect of charge transfer in DNA [36].

In the next section we address the system dynamics at temperatures above the environment melting point, when the PBH model is more appropriate.

D. Room temperature: Mixed regime

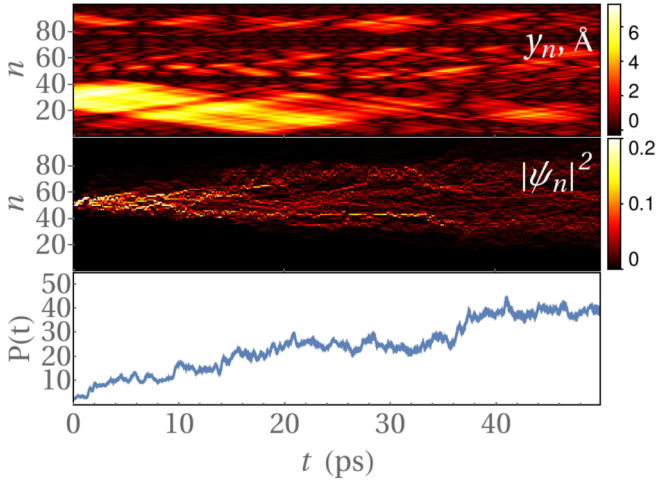
In this section we study the most relevant case of high temperatures: Above the medium melting point but still well below the critical one (the denaturation temperature). Results of our calculation of one particular typical system trajectory for $T = 300$ K are presented in Fig. 12. One can see from the upper panel that the characteristic displacements are on the order of an \AA , in which case the interaction potential $W(y_n, y_{n+1})$ (negligible for small displacements) starts playing an important role. This manifests itself in the appearance of very specific strong fluctuations: Chunks of several sites moving in a correlated way (for example, in phase). These chunks are substantially heavier than a single base, so their dynamics is slower and, as the panel suggests, they can be very long living. See, for example, the brighter yellow

FIG. 13. Same as in Fig. 9 but for $T = 300$ K. Solid red line gives the best power law fit to the data within the region $t > 10$ ps, while the gray line—in the region $t < 10$ ps.

traces showing such fluctuations around $n \approx 20$ – 30 and $n \approx 60$ – 70 . Their characteristic period is on the order of several ps. Note also that the part of the figure enclosed between them is considerably darker which corresponds to smaller stretchings. This means that with respect to that enclosed part, the two stronger fluctuations act as much higher potential barriers for electron wave packet. Indeed, from the electron density dynamics (see the middle panel) one can see that the wave packet is visibly confined between the two trains of oscillating high barriers for a very long time: Until about $t \approx 20$ – 30 ps. The resulting slow-down of the wave packet spreading is also reflected in the behavior of the PN (see the lower panel) and the dynamics of the packet width.

Figure 13 shows the time dependence of the ensemble averaged packet width calculated for a chain of $N = 1000$ sites and $T = 300$ K. Two different transfer regimes can be distinguished in the figure: For $t < 10$ ps and $t > 10$ ps. Gray and red solid lines give the best power law fits to the numerical data within the two time ranges. As expected, the packet expansion is diffusive in the long time limit (with the exponent of 0.5). At this temperature the fluctuations governing the charge transfer have characteristic space and timescales, which set natural timescales for the random walk process. From the upper panel of Fig. 12 the following estimations can be made: The typical spacing between adjacent *strong* fluctuations is on the order of 10 lattice constants and their period is on the order of several ps. Only when the propagation time substantially exceeds such a timescale, the diffusive nature of the propagation can manifest itself. The latter agrees well with $t \sim 10$ ps being the time separating the two regimes in this case. Strong fluctuations split the chain into chunks which appear to act as new “supersites.” The size of the latter gives the characteristic length scale of the random walk on a chain of such supersites. This is also in agreement with the fact that the diffusive spreading starts when $\sigma(t) > 10$ (which happens at $t \approx 10$ ps). We can argue therefore that the diffusive regime is governed by space and time characteristics of *large* fluctuations.

For shorter times ($t < 10$ ps) the packet dynamics is clearly subdiffusive with the exponent of about 0.37. The latter can

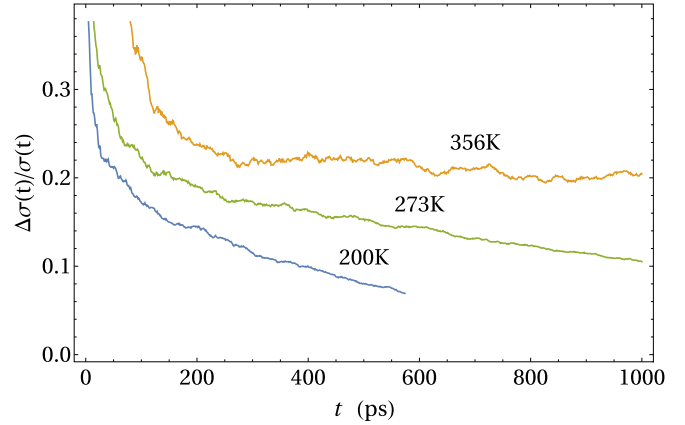
FIG. 14. Same as in Fig. 8 but for $T = 340$ K.

be explained by the fact that the wave packet is efficiently confined by neighboring strong and long-living fluctuations (as we have discussed above), which traps the charge density within a limited chunk of the whole DNA chain for substantially long time, resulting in a slowing down of the overall packet dynamics and making it subdiffusive within this time range. We can conclude that the charge transfer in DNA at room temperature is subdiffusive up to about 10 ps during which a wave packets spreads over about 10–20 base pairs.

We checked that the lattice dynamics does not change if the vibrational and the electronic parts of the system are decoupled (results not shown here), suggesting that the influence of the charge dynamics on the vibrational one is negligible. Therefore, we can conclude that, within the PBH model, the polaronic effect is irrelevant for the charge transfer in DNA at close to room temperatures. Contrary to that, the electron-phonon interaction is determinant for the charge dynamics because charge transfer is governed by the lattice fluctuations; such a mechanism can be called the fluctuation-governed charge transfer.

E. Close to critical temperatures: Subdiffusive regime

In this section we address briefly a very special case in which the system is close to its phase transition point. Within the considered model the melting transition temperature is about 356 K [60,61]. Results of our calculation for one particular system trajectory at $T = 340$ K are presented in Fig. 14. It is known that in the vicinity of a phase transition point fluctuations become critical or scale-free, which means that both small and very large (diverging at the transition) fluctuations can coexist. In the case of DNA such large fluctuations correspond to so called bubbles [85]—large openings in the double helix chain—resulting finally in the DNA denaturation or melting, i.e., complete separation of the two strands. In the PBH model the melting corresponds to divergence of the H-bond stretchings y_n . The upper panel of the figure demonstrates fluctuations of very different sizes—a precursor of the scale-free or critical ones. They can be very long living and therefore, as we have argued above, the wave packet can

FIG. 15. Relative fluctuation of the wave packet width: The ratio of the standard deviation $\Delta\sigma(t)$ of the packet width $\sigma(t)$ to the width itself calculated for different temperatures indicated in the plot. The system size is $N = 1000$ (in all cases $\sigma(t) \ll N$, so size effects are negligible).

be confined efficiently by them for considerable amounts of time. The result of such strong confinement can be clearly seen in the middle and the lower panel of the figure. Note, in particular, that the PN has flat plateaus, for example, for $5 \lesssim t \lesssim 10$ or $20 \lesssim t \lesssim 35$ corresponding to time windows when the wave packet is localized between a pair of bubbles. The characteristic space and timescales of the charge dynamics are determined by those of the chain fluctuations. Due to the criticality of fluctuations at the transition point they are scale free both in space and time and therefore the charge dynamics can be expected to manifest anomalous behavior. We observed a subdiffusive wave packet dynamics with $\sigma(t) \sim t^{0.48}$ for the critical temperature $T = 356$ K. However, a direct study of such a dynamics in more detail would require very large size and timescale calculations. An alternative way to detect anomalous transport properties relies on properties of fluctuations. For example, one can address the relative fluctuation of the wave packet size. At the transition point, both the size and its fluctuation is expected to grow at the same rate in the thermodynamic limit, so their ratio should tend to a constant (see, e.g., Ref. [86] and references therein). Below we use the latter approach to demonstrate the anomalous character of the diffusion. To illustrate the emergence of the anomalous regime of the charge transfer at the transition temperature we plot in Fig. 15 the evolution of the ratio $\Delta\sigma(t)/\sigma(t)$ of the standard deviation of the electronic wave packet size to the size itself, calculated for different temperatures. For temperatures well below the critical one ($T = 200$ K and $T = 273$ K) such relative size fluctuation is decaying with time, which reflects the fact that the role of fluctuations decreases and the expanding wave packet has a well defined size. Contrary to that, at the critical temperature, $T = 356$ K, the relative fluctuation tends to a constant, indicating that the fluctuations of the wave packet size remain on the order of the size itself in the thermodynamic limit—a typical feature of critical states and anomalous transport regimes. The latter supports our claim on the anomalous character of diffusion close to the denaturation transition point. A more detailed analysis of this case goes far beyond the scope of the present work.

F. On possible impacts of the base sequence inhomogeneity and initial conditions

Here we briefly discuss possible impacts of the base pair sequence inhomogeneity and different initial conditions (injection of an electron in a site different from the central one) on our results.

In this work we considered a homogeneous base pair sequence which can be seen as a considerable limitation of the model. From the point of view of the charge transfer or transport the most relevant differences in base pairs parameters are probably those in the base (site) energies, which would introduce large on-site static disorder and determine the charge transfer efficiency and transport properties at low temperatures (see, for example, Refs. [21,52–55] and references therein). However, as we argue above, the applicability of the PBH model at such temperatures is questionable anyway. At high temperatures (above the environment melting point), the typical value of the positive bond stretching y_n is on the order of few angstrom (that can be estimated from Figs. 12, 14), therefore the characteristic scale of the diagonal energy dynamic fluctuation is greater than 1 eV which is on the order of or exceeding the differences between base energies. We believe that the latter should reduce the impact of the site energy differences on the transfer. A more detailed quantitative comparison would require a separate extensive study, which goes beyond the scope of the present work.

In the current section we used the following initial condition: An electron was created (injected) at the central site while in reality it can be injected in an arbitrary one. This could have some impact on final results. However, the time evolution of all studied quantities was calculated by averaging over many random trajectories. For each trajectory an electron is injected into a completely random energy potential. Taking into account our previous argument, the typical fluctuations of the potential energy at high temperatures are largely governed by the dynamic fluctuations of the chain. This suggests that injecting an electron into a different site is most probably equivalent (from the point of view of the final averaged result, at least) to injecting it into the center of another realization of the thermalized chain configuration. Therefore, it probably would not have any substantial impact on averaged results.

G. On the relationship with variable-range hopping models

We have argued in the previous sections that the charge transfer mechanisms within the considered model intrinsically involve different time and size scales; the latter, in particular, can resemble the variable-range hopping mechanism [87–89] originally proposed to describe low-temperature hopping conductivity in semiconductors [90]. Similar mechanisms were discussed in the framework of the energy transfer in J-aggregates [82–84]; those were based on the idea of the hidden energy structure in the density of quasiparticle states [76,77,79,80]. Variable-range hopping of polarons was also proposed to explain the charge transfer in DNA [30,32,37]. We note however that, despite the seeming similarity, those mechanisms rely on the static characteristics of the system, while our proposed charge transfer mechanisms rely on dynamical fluctuations and size and timescales which are of key importance for the explanation of the system dynamics

and charge transfer. Therefore, our proposed fluctuation-governed mechanism is considerably different from those discussed in previous studies.

VI. CONCLUSIONS

We have studied various mechanisms and regimes of the charge transfer in the DNA molecules within the framework of the Peyrard-Bishop-Holstein model which considers coupled dynamics of the electronic and vibrational degrees of freedom of the system. At zero temperature the minimum energy configuration of the model is polaronic. For this reason, first, we analyzed the polaron dynamics *during* the DNA chain thermalization by connecting the system with a formed polaron (at zero temperature) to a heat bath having a finite temperature $T_0 > 0$ and letting the system thermalize completely. We found that for such initial condition the polaron has a finite lifetime in the whole range of studied temperatures, $T_0 \approx 10$ –356 K. More importantly, the polaron breaks up long before the vibrational subsystem reaches the equilibrium at the temperature of the bath. We believe that the latter result suggests that the polaron charge transfer mechanism is irrelevant within the framework of the PBH model because a polaron does not seem to be a stable configuration within the considered temperature range.

Second, we studied the system dynamics under a more realistic initial condition: A charge injected into a thermalized DNA chain. We found no traces of polaron formation either. Rather, we observed and analyzed a variety of charge transfer regimes within different temperature ranges. We show that the charge transfer is quasiballistic at low temperatures: A wave packet can expand almost ballistically over several dozens of system sites (base pairs). We argue also that for temperatures that are below the environment (bath) freezing point, the applicability of the PBH model is questionable because the typical large displacements in the vibrational subsystem can hardly be realistic in a glassy host medium.

We demonstrated that for temperatures above the environment melting point (i.e., in the case of a liquid environment), which is the most interesting and relevant temperature range for real biological systems, the charge transfer regime is mixed: Subdiffusive at short times and diffusive in the long time limit, provided that the temperature is not too close to the DNA melting (denaturation) point. Despite the fact that the diffusive charge transfer can naturally be expected, its mechanism is quite peculiar. Due to the electron-phonon interaction, positive displacements in the vibrational subsystem (stretchings of H-bonds) act as potential barriers for the charge, so that the latter can be efficiently confined between two neighboring fluctuations during substantial part of their oscillation periods. Thus, the vibrational subsystem sets a clock for the electronic one and determines the regime of the charge transfer. In other words, the dynamics of the charge density is governed by that of the vibrational subsystem: We call such a mechanism of charge transfer fluctuation-governed. As long as the mechanical subsystem fluctuations have finite size and timescales, the charge transfer regime is diffusive in the long time limit. At shorter times which are on the order of the characteristic timescale of the vibrational subsystem (few ps at 300 K), the charge transfer regime is subdiffusive.

Finally, as the temperature approaches the critical one, at which DNA undergoes the denaturation phase transition, mechanical fluctuations become scale free. We argued that in this case the charge transfer becomes anomalous, in particular, subdiffusive even in the long time limit.

Summarizing, we note that we considered a particular model of an organic macromolecular system in which electronic and vibrational degrees of freedom are strongly coupled due to a very specific mechanical deformations: The stretching y_n of the H-bond between two DNA bases within a pair. However, the electron-phonon coupling term employed in the model Hamiltonian has a very generic form. Therefore, for another system, y_n can represent a very different generalized or phenomenological coordinate characterizing the dynamics of the vibrational subsystem. Then within the Holstein approximation the Hamiltonian of the considered system would be very similar, leaving our qualitative reasoning valid. We believe therefore that our proposed mechanism of fluctuation-governed charge transfer can be relevant for

other organic systems with strong electron-phonon coupling, such as, the conjugated polymers, molecular aggregates, α -helices, β -sheets, etc.

ACKNOWLEDGMENTS

This work was partially supported by CNPq, CAPES (Grant No. PVE-A121) and FINEP (Federal Brazilian Agencies), as well as FAPEAL (Alagoas State Agency) and Spanish MINECO Grants No. MAT2013-46308 and No. MAT2016-75955. A.V.M. is grateful to the Universidade Federal de Alagoas (where a part of this work has been carried out) for hospitality. R.P.A.L. is grateful to the Universidad Complutense de Madrid and Warwick University (where a part of this work has been carried out) for hospitality. The authors also thank V. A. Malyshev for critical reading of the manuscript and acknowledge the crucial contribution of J. Munárriz to numerical calculations of the system dynamics.

-
- [1] J. D. Watson and F. H. Crick, *Nature (London)* **171**, 737 (1953).
 - [2] R. G. Endres, D. L. Cox, and R. R. P. Singh, *Rev. Mod. Phys.* **76**, 195 (2004).
 - [3] T. Chakraborty (Ed.), *Charge Migration in DNA*, NanoScience and Technology (Springer, Berlin, 2007)
 - [4] C. Murphy, M. Arkin, Y. Jenkins, N. Ghatlia, S. Bossmann, N. Turro, and J. Barton, *Science* **262**, 1025 (1993).
 - [5] E. Braun, Y. Eichen, U. Sivan, and G. Ben-Yoseph, *Nature (London)* **391**, 775 (1998).
 - [6] A. J. Storm, J. van Noort, S. de Vries, and C. Dekker, *Appl. Phys. Lett.* **79**, 3881 (2001).
 - [7] K.-H. Yoo, D. H. Ha, J.-O. Lee, J. W. Park, J. Kim, J. J. Kim, H.-Y. Lee, T. Kawai, and H. Y. Choi, *Phys. Rev. Lett.* **87**, 198102 (2001).
 - [8] G. Cuniberti, L. Craco, D. Porath, and C. Dekker, *Phys. Rev. B* **65**, 241314(R) (2002).
 - [9] Xu, Zhang, Li, and Tao, *Nano Lett.* **4**, 1105 (2004).
 - [10] H. Cohen, C. Noguees, R. Naaman, and D. Porath, *Proc. Natl. Acad. Sci. USA* **102**, 11589 (2005).
 - [11] Y. Okahata, T. Kobayashi, K. Tanaka, and M. Shimomura, *J. Am. Chem. Soc.* **120**, 6165 (1998).
 - [12] H.-W. Fink and C. Schönberger, *Nature (London)* **398**, 407 (1999).
 - [13] A. Rakitin, P. Aich, C. Papadopoulos, Y. Kobzar, A. S. Vedeneev, J. S. Lee, and J. M. Xu, *Phys. Rev. Lett.* **86**, 3670 (2001).
 - [14] O. Legrand, D. Côte, and U. Bockelmann, *Phys. Rev. E* **73**, 031925 (2006).
 - [15] F. Charra, V. M. Agranovich, and F. Kajzar (Eds.), *Organic Nanophotonics* (Springer, Dordrecht, 2003).
 - [16] E. Díaz, A. V. Malyshev, and F. Domínguez-Adame, *Phys. Rev. B* **76**, 205117 (2007).
 - [17] S. Sönmezoglu and Ö. A Sönmezoglu, *Mater. Sci. Eng. C* **31**, 1619 (2011).
 - [18] J. B. Schimelman, D. M. Dryden, L. Poudel, K. E. Krawiec, Y. Ma, R. Podgornik, V. A. Parsegian, L. K. Denoyer, W.-Y. Ching, N. F. Steinmetz, and R. H. French, *Phys. Chem. Chem. Phys.* **17**, 4589 (2015).
 - [19] D. Porath, A. Bezryadin, S. de Vries, and C. Dekker, *Nature (London)* **403**, 635 (2000).
 - [20] E. Díaz, R. P. A. Lima, and F. Domínguez-Adame, *Phys. Rev. B* **78**, 134303 (2008).
 - [21] E. Albuquerque, U. Fulco, V. Freire, E. Caetano, M. Lyra, and F. de Moura, *Phys. Rep.* **535**, 139 (2014).
 - [22] J. S. Hwang, K. J. Kong, D. Ahn, G. S. Lee, D. J. Ahn, and S. W. Hwang, *Appl. Phys. Lett.* **81**, 1134 (2002).
 - [23] E. Maciá, *Phys. Rev. B* **80**, 125102 (2009).
 - [24] J. H. Ojeda, R. P. A. Lima, F. Domínguez-Adame, and P. A. Orellana, *J. Phys.: Condens. Matter* **21**, 285105 (2009).
 - [25] G. Torrellas and E. Maciá, *Phys. Lett. A* **376**, 3407 (2012).
 - [26] A. V. Malyshev, *Phys. Rev. Lett.* **98**, 096801 (2007).
 - [27] G. Kalosakas, K. Rasmussen, and A. R. Bishop, *J. Chem. Phys.* **118**, 3731 (2003).
 - [28] P. Maniadis, G. Kalosakas, K. O. Rasmussen, and A. R. Bishop, *Phys. Rev. B* **68**, 174304 (2003).
 - [29] M. A. Fuentes, P. Maniadis, G. Kalosakas, K. O. Rasmussen, A. R. Bishop, V. M. Kenkre, and Y. B. Gaididei, *Phys. Rev. E* **70**, 025601(R) (2004).
 - [30] M. R. Singh, *J. Biomater. Sci. Polym. Ed.* **15**, 1533 (2004).
 - [31] P. Maniadis, G. Kalosakas, K. O. Rasmussen, and A. R. Bishop, *Phys. Rev. E* **72**, 021912 (2005).
 - [32] M. R. Singh, *Phys. Status Solidi (c)* **2**, 2970 (2005).
 - [33] E. B. Starikov, *Philos. Mag.* **85**, 3435 (2005).
 - [34] R. Gutiérrez, S. Mohapatra, H. Cohen, D. Porath, and G. Cuniberti, *Phys. Rev. B* **74**, 235105 (2006).
 - [35] J. H. Wei, X. J. Liu, J. Berakdar, and Y. Yan, *J. Chem. Phys.* **128**, 165101 (2008).
 - [36] A. V. Malyshev, E. Díaz, F. Domínguez-Adame, and V. A. Malyshev, *J. Phys.: Condens. Matter* **21**, 335105 (2009).
 - [37] M. R. Singh, G. Bart, and M. Zinke-Allmang, *Nanoscale Res. Lett.* **5**, 501 (2010).
 - [38] G. Kalosakas, *Phys. Rev. E* **84**, 051905 (2011).
 - [39] T. Y. Astakhova, V. A. Kashin, V. N. Likhachev, and G. A. Vinogradov, *Russ. J. Phys. Chem. A* **88**, 1945 (2014).
 - [40] A. P. Chetverikov, W. Ebeling, V. D. Lakhno, A. S. Shigaev, and M. G. Velarde, *Eur. Phys. J. B* **89**, 101 (2016).

- [41] Z. G. Yu and X. Song, *Phys. Rev. Lett.* **86**, 6018 (2001).
- [42] S. S. Alexandre, E. Artacho, J. M. Soler, and H. Chacham, *Phys. Rev. Lett.* **91**, 108105 (2003).
- [43] S. Komineas, G. Kalosakas, and A. R. Bishop, *Phys. Rev. E* **65**, 061905 (2002).
- [44] J. D. Slinker, N. B. Muren, S. E. Renfrew, and J. K. Barton, *Nat. Chem.* **3**, 228 (2011).
- [45] S. O. Kelley and J. K. Barton, *Science* **283**, 375 (1999).
- [46] D. Rawtani, B. Kuntmal, and Y. Agrawal, *Front. Life Sci.* **9**, 214 (2016).
- [47] R. E. Holmlin, P. J. Dandliker, and J. K. Barton, *Angew. Chem. Int. Ed. Engl.* **36**, 2714 (1997).
- [48] M. Fujitsuka and T. Majima, *Pure Appl. Chem.* **85**, 1367 (2013).
- [49] L. Vidmar, J. Bonča, M. Mierzejewski, P. Prelovšek, and S. A. Trugman, *Phys. Rev. B* **83**, 134301 (2011).
- [50] N. K. Voulgarakis, *Phys. B: Condens. Matter* **519**, 15 (2017).
- [51] V. Giorgis, A. Malyshev, and V. Malyshev, Book of Abstracts: 19th International Conference on Dynamical Processes in Excited States of Solids (2016).
- [52] E. L. Albuquerque, M. S. Vasconcelos, M. L. Lyra, and F. A. B. F. de Moura, *Phys. Rev. E* **71**, 021910 (2005).
- [53] C. J. Páez, P. A. Schulz, N. R. Wilson, and R. A. Römer, *New J. Phys.* **14**, 093049 (2012).
- [54] K. Lambropoulos, M. Chatzieftheriou, A. Morphis, K. Kaklamanis, M. Theodorakou, and C. Simserides, *Phys. Rev. E* **92**, 032725 (2015).
- [55] K. Lambropoulos, M. Chatzieftheriou, A. Morphis, K. Kaklamanis, R. Lopp, M. Theodorakou, M. Tassi, and C. Simserides, *Phys. Rev. E* **94**, 062403 (2016).
- [56] V. N. Likhachev, O. I. Shevaleevskii, and G. A. Vinogradov, *Chin. Phys. B* **25**, 018708 (2016).
- [57] A. A. Voityuk, K. Siriwong, and N. Rösch, *Phys. Chem. Chem. Phys.* **3**, 5421 (2001).
- [58] H. A. Wagenknecht and H. B. Gray, *Charge Transfer in DNA: From Mechanism to Application*, edited by H.-A. Wagenknecht (Wiley-VCH Verlag GmbH & Co. KGaA, Weinheim, FRG, 2005), p. 245.
- [59] J. C. Genereux and J. K. Barton, *Chem. Rev.* **110**, 1642 (2010).
- [60] M. Peyrard and A. R. Bishop, *Phys. Rev. Lett.* **62**, 2755 (1989).
- [61] T. Dauxois, M. Peyrard, and A. R. Bishop, *Phys. Rev. E* **47**, R44 (1993).
- [62] T. D. Amarante and G. Weber, *J. Phys.: Conf. Ser.* **490**, 012203 (2014).
- [63] J. P. Peters, S. P. Yelgaonkar, S. G. Srivatsan, Y. Tor, and I. James Maher, L., *Nucleic Acids Res.* **41**, 10593 (2013).
- [64] R. A. Suris, *J. Exptl. Theoret. Phys.* **47**, 1427 (1965).
- [65] R. A. Suris, *Sov. Phys. JETP* **20**, 961 (1965).
- [66] L. D. Landau and S. I. Pekar, *Zh. Eksp. Teor. Fiz.* **18**, 419 (1948).
- [67] L. D. Landau and S. I. Pekar, in *Collected Papers of L.D. Landau*, 5 (Elsevier, Amsterdam, 1965), pp. 478–483.
- [68] T. Dauxois, M. Peyrard, and A. R. Bishop, *Phys. Rev. E* **47**, 684 (1993).
- [69] Y. Gao, K. V. Devi-Prasad, and E. W. Prohofsky, *J. Chem. Phys.* **80**, 6291 (1984).
- [70] A. Campa and A. Giansanti, *Phys. Rev. E* **58**, 3585 (1998).
- [71] C. W. Gardiner, U. N. Bhat, D. Stoyan, D. J. Daley, Y. a. Kutoyants, and B. L. S. P. Rao, *Biometrics*, Vol. 42 (Springer-Verlag, Berlin, 1986), p. 226.
- [72] E. Helfand, *Bell Sys. Tech. J.* **58**, 2289 (1979).
- [73] H. S. Greenside and E. Helfand, *Bell Sys. Tech. J.* **60**, 1927 (1981).
- [74] V. A. Malyshev, *Opt. Spectrosc.* **84**, 195 (1998).
- [75] L. D. Landau and E. M. Lifshitz, *Mechanics* (Pergamon Press, Oxford, UK, 1969).
- [76] V. Malyshev, *Opt. Spektrosk.* **71**, 873 (1991).
- [77] V. Malyshev, *Opt. Spectrosc.* **71**, 505 (1991).
- [78] V. Malyshev, *J. Lum.* **55**, 225 (1993).
- [79] V. Malyshev and P. Moreno, *Phys. Rev. B* **51**, 14587 (1995).
- [80] A. V. Malyshev and V. A. Malyshev, *Phys. Rev. B* **63**, 195111 (2001).
- [81] A. Malyshev and V. Malyshev, *J. Lum.* **94-95**, 369 (2001).
- [82] A. V. Malyshev, V. A. Malyshev, and F. Domínguez-Adame, *Chem. Phys. Lett.* **371**, 417 (2003).
- [83] A. V. Malyshev, V. A. Malyshev, and F. Domínguez-Adame, *J. Phys. Chem. B* **107**, 4418 (2003).
- [84] A. V. Malyshev, V. A. Malyshev, and J. Knoester, *Phys. Rev. Lett.* **98**, 087401 (2007).
- [85] G. Altan-Bonnet, A. Libchaber, and O. Krichevsky, *Phys. Rev. Lett.* **90**, 138101 (2003).
- [86] A. V. Malyshev, V. A. Malyshev, and F. Domínguez-Adame, *Phys. Rev. B* **70**, 172202 (2004).
- [87] N. F. Mott, *Philos. Mag.* **19**, 835 (1969).
- [88] A. L. Efros and B. I. Shklovskii, *J. Phys. C: Solid State Phys.* **8**, L49 (1975).
- [89] B. I. Shklovskii and A. L. Efros, *Electronic Properties of Doped Semiconductors*, Springer Series in Solid-State Sciences, Vol. 45 (Springer, Berlin, 1984).
- [90] The Efros-Shklovskii variable-range hopping model [88,89] was also successfully applied to describe some aspects of charge transport in DNA (see, for example, Ref. [30]).